

# Generating Single Microwave Photons in a Circuit

A. A. Houck\*,<sup>1</sup> D. I. Schuster\*,<sup>1</sup> J. M. Gambetta,<sup>1</sup> J. A. Schreier,<sup>1</sup> B. R. Johnson,<sup>1</sup>  
J. M. Chow,<sup>1</sup> J. Majer,<sup>1</sup> L. Frunzio,<sup>1</sup> M. H. Devoret,<sup>1</sup> S. M. Girvin,<sup>1</sup> and R. J. Schoelkopf<sup>1</sup>

<sup>1</sup>*Departments of Applied Physics and Physics, Yale University, New Haven, CT 06520*

(Dated: November 26, 2024)

Electromagnetic signals in circuits consist of discrete photons[1], though conventional voltage sources can only generate classical fields with a coherent superposition of many different photon numbers. While these classical signals can control and measure bits in a quantum computer (qubits), single photons can carry quantum information, enabling non-local quantum interactions, an important resource for scalable quantum computing[2]. Here, we demonstrate an on-chip single photon source in a circuit quantum electrodynamics (QED) architecture[3], with a microwave transmission line cavity that collects the spontaneous emission of a single superconducting qubit with high efficiency. The photon source is triggered by a qubit rotation, as a photon is generated only when the qubit is excited. Tomography of both qubit and fluorescence photon shows that arbitrary qubit states can be mapped onto the photon state, demonstrating an ability to convert a stationary qubit into a flying qubit. Both the average power and voltage of the photon source are characterized to verify performance of the system. This single photon source is an important addition to a rapidly growing toolbox for quantum optics on a chip.

Numerous approaches to generating single photons, particularly optical photons, have been proposed and demonstrated in recent years[4]. The underlying principle for generating single photons from atoms or qubits is straightforward: an excited qubit can relax to its ground state by emitting a photon[5, 6]. A pulse that excites the qubit can therefore trigger a single photon emission, as long as the control and emission photons can be separated. Early experiments demonstrated this photon generation from single ions[7], atoms[8], molecules[9, 10, 11], nitrogen vacancies[12], and quantum dots[13, 14], though radiation in all directions made efficient collection difficult. In a cavity QED source, the atom or qubit is coupled to a single photonic mode of a cavity, enhancing the rate of decay to that mode through the Purcell effect[15] and allowing a source where photons are emitted into a controlled channel. Atoms [16, 17, 18, 19], ions [20], and quantum dots[14, 21, 22] have been used to generate optical photons efficiently in this manner.

Here, we implement a cavity QED system in a circuit[23, 24], where a superconducting qubit and transmission line cavity are coupled such that the dominant channel for relaxation of the qubit is to spontaneously emit a photon into the cavity. Each time the qubit is excited, the most likely outcome is the generation of one (and only one) photon at a random time, with the distribution of times characterized by the decay rate of the qubit. The challenge is to create a system where spontaneous emission dominates other relaxation channels. This spontaneous emission rate can be determined from the Hamiltonian of the system, the well-known Jaynes-Cummings Hamiltonian,  $H = \hbar\omega_a\sigma_z/2 + \hbar\omega_r(a^\dagger a + 1/2) +$

$\hbar g(a^\dagger\sigma^- + a\sigma^+)$ . The first two terms represent a qubit with frequency  $\omega_a$  described by Pauli operators  $\sigma_x$ ,  $\sigma_y$ , and  $\sigma_z$  and raising and lowering operators  $\sigma^+$  and  $\sigma^-$ , and a single photon mode of frequency  $\omega_r$  described by the photon operators  $a$  and  $a^\dagger$ . The final term represents a coupling of strength  $g$  between the qubit and the photon, which mixes the individual qubit and photon eigenstates. When far detuned ( $\Delta = \omega_r - \omega_a \gg g$ ), the qubit acquires a small photonic component of the wavefunction, of magnitude  $g/\Delta$ . This opens a new source of decay for the qubit, as the photonic component of the qubit can decay at the cavity decay rate,  $\kappa$ , resulting in a new qubit decay rate  $\gamma_\kappa = (g/\Delta)^2\kappa$ . The qubit can be an efficient photon source if this new decay rate dominates over other non-radiative decay rates,  $\gamma_\kappa > \gamma_{NR}$ .

Verifying the single photon output is a substantial challenge in on-chip microwave experiments. The simplest approach, looking for a photon each time one is created, is not possible; unlike in optical frequency experiments, no detectors can yet resolve single microwave photon events in a single shot. Fortunately, several unique characteristics of the source are evident in the average signal generated by many single photon events, together yielding a convincing verification even with noisy detectors. Most simply, the output of the single photon source is expected to be oscillatory in the amplitude of the control pulse applied to rotate the qubit. Second, the average amplitude produced should agree well with the expected value for a single photon. Finally, and most importantly, if the output of the system depends only on the state of the qubit, state tomography measured for the photons should show complete agreement with that obtained from independent measurements of the qubit. The source reported here meets all three of these criteria.

The circuit designed to generate photons consists of a superconducting transmon qubit[25], an optimized ver-

---

\*Authors with contributed equally to this work.

sion of the Cooper Pair Box[26], capacitively coupled to a half-wave transmission line cavity with fundamental frequency  $\omega_r/2\pi = 5.19$  GHz (see Figure 1). Two important design differences between this circuit and previous incarnations of circuit QED[23] are needed to achieve efficient single photon generation. First, the cavity is asymmetric in that the capacitors (mirrors) at either end of the transmission line are no longer equal, resulting in asymmetric decay rates to the input and output ports ( $\kappa_{\text{in}}/2\pi \approx 200$  kHz for the input side and  $\kappa_{\text{out}}/2\pi = 44$  MHz for the output). As a result, photons generated in the cavity are emitted at the output port more than 99% of the time. In addition, the total decay rate for the cavity,  $\kappa/2\pi = 44$  MHz, is substantially higher than in previous samples, a necessary change for spontaneous emission to be the dominant relaxation channel for the qubit. The qubit decay rate in the absence of spontaneous emission,  $\gamma_{\text{NR}}$ , is frequency dependent, with  $\gamma_{\text{NR}}/2\pi < 2$  MHz for all measured trans-

mission frequencies between 4.3 and 7.3 GHz.

Transmission measurements are used to probe the energy spectrum of this system while the qubit frequency is tuned via an external magnetic field (see Figure 2). When the qubit is far detuned from the cavity, only a single transmission peak is observed, centered at the cavity frequency with a Lorentzian lineshape and width given by the bare cavity width. When the qubit and cavity are resonant, two peaks in transmission are seen, a phenomenon known as the vacuum Rabi splitting. Each peak corresponds to one of the two single-excitation eigenstates of the system, superpositions of the separate qubit and photon excitation states. The width of each peak is the average of the qubit and photon decay rates,  $(\gamma + \kappa)/2$ . In the dispersive limit, where the detuning  $\Delta$  is much larger than the coupling  $g$ , spontaneous emission is enhanced by the Purcell effect[15], resulting in approximate decay rates  $[1 - (g/\Delta)^2]\kappa + (g/\Delta)^2\gamma$  and  $[1 - (g/\Delta)^2]\gamma + (g/\Delta)^2\kappa$ . Experimentally determined linewidths agree well with

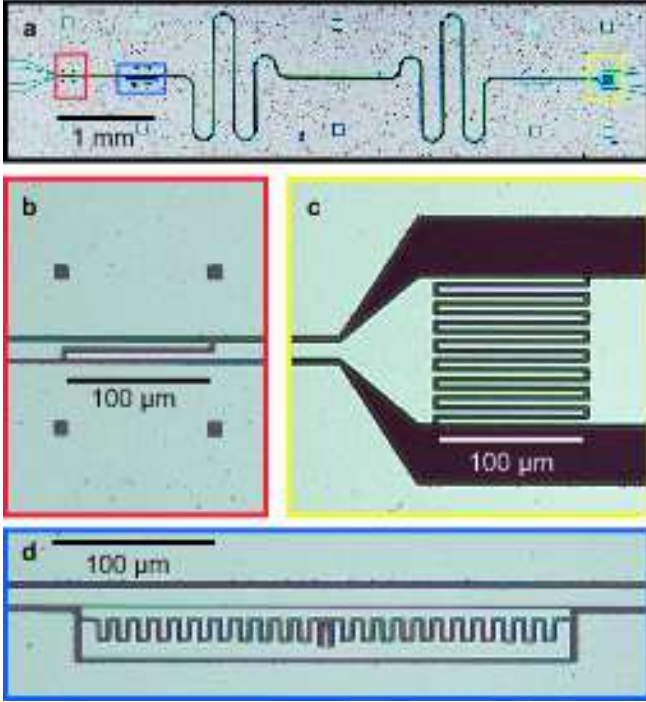


FIG. 1: The circuit QED device for generating single photons. **a.** A transmission line cavity is formed between two capacitors, with the input capacitor shown in **b** and the output in **c**. Because the output is much larger, most radiation leaving the cavity leaves from this port, allowing efficient collection of light emitted from the cavity. **d.** Transmon qubit, an optimized Cooper Pair Box, at a voltage anti-node of the cavity. The qubit is characterized by a Josephson energy  $E_J^{\text{max}} = 20.2$  GHz and a charging energy  $E_c = 0.37$  GHz. The coupling to the cavity is  $g = 107$  MHz at the qubit frequency primarily used in this paper,  $\omega_a = 4.68$  GHz, and has a slight dependence on the qubit frequency.

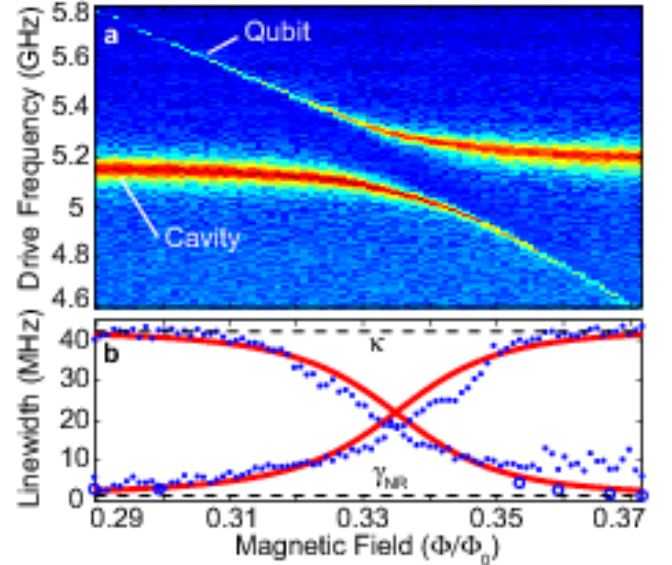


FIG. 2: Enhanced spontaneous emission through the Purcell effect. **a.** Transmission through the cavity-qubit system at different applied fluxes (log scale). Two peaks are evident in transmission due to the vacuum Rabi splitting. Away from the avoided crossing, these peaks correspond to “mostly qubit” and “mostly cavity” states. The bare linewidth of the cavity,  $\kappa/2\pi = 44$  MHz, is much larger than the bare qubit linewidth  $\gamma/2\pi < 2$  MHz. **b.** Extracted linewidths from the data in (a) (closed circles) are compared with theoretical values (red line). As the qubit and cavity peaks approach degeneracy, the qubit peak becomes broader due to spontaneous emission to the cavity mode, while the cavity decay is suppressed. Extra dephasing present only at low frequencies (the right side of the graph) causes a non-Lorentzian line shape and excessive width. Measurements of the relaxation rate in the time domain (open circles) agree with theoretical estimates. Discrepancies arise due to flux instability and variations in non-radiative decay with frequency.

theoretical predictions (Figure 2b), demonstrating an ability to tune the rate of radiative decay of the qubit by tuning its frequency.

It is this enhanced qubit decay due to the cavity that is utilized in generating single photons: the qubit line broadens when the decay of the photon-like part of the wavefunction dominates the non-radiative qubit decay. For the results presented here, the qubit was tuned to a frequency  $\omega_a/2\pi = 4.68$  GHz. With a coupling  $g/2\pi = 107$  MHz, the qubit wave functions had a  $(g/\Delta)^2 = 4\%$  photonic nature, resulting in a spontaneous emission rate  $\gamma_\kappa/2\pi = 1.9$  MHz. The measured relaxation rate of the qubit was  $\gamma/2\pi = 1.8 \pm 0.1$  MHz, indicating that the observed relaxation could be mostly accounted for by spontaneous emission to the cavity to within our measurement accuracy. Because the lifetime of the qubit is short, the photon source is effectively reset in under  $1 \mu\text{s}$ , allowing for rapid repeated photon generation, for a peak source power of 3 aW.

To verify single photon generation, we first show that the output of the cavity is an oscillatory function of the input drive, as at most one photon is generated regardless of the magnitude of the input drive. A 12 ns Gaussian control pulse rotates the qubit state by a Rabi angle that is proportional to the pulse amplitude. The excited qubit will relax, generating a new photon state at the qubit frequency. Because the control pulse leaves the cavity at a rate that is much faster than the rate of spontaneous emission  $\gamma_\kappa$ , the control pulse and generated photons can easily be separated in time. As seen in Figure 3a, the measured control signal increases monotonically, while the spontaneous emission oscillates as the qubit is rotated through from the ground to the excited state and back, confirming that the spontaneous emission is proportional to the qubit state, not simply the applied drive amplitude. This is the key to the experiment: a superposition of many photons incoming on one temporal mode give rise to one and only one photon on a distinct outgoing temporal mode. Moreover, because a single photon is the maximum output, the source is to first order insensitive to fluctuations in the control pulse when generating one photon.

We characterize both the power and electric field of the single photon source, using independent measurements of the qubit state made with dispersive readout techniques[27] to verify performance (Figure 3). If the qubit state is mapped to the photon state, then an arbitrary superposition of the ground and excited states  $\alpha|g\rangle + \beta|e\rangle$  will result in the same superposition of photon states:  $\alpha|0\rangle + \beta|1\rangle$ , where  $|0\rangle$  and  $|1\rangle$  refer to states with zero or one photon. The average photon number is proportional to the average qubit excitation probability,  $\langle a^\dagger a \rangle = (\langle \sigma_z \rangle + 1)/2$ , which has a maximum of one photon when the qubit is in the purely excited state. The two quadratures of homodyne voltage, on the other hand, are proportional to the x and y-components of the

qubit state:  $\langle a + a^\dagger \rangle = \langle \sigma_x \rangle$  and  $i\langle a^\dagger - a \rangle = \langle \sigma_y \rangle$ . The measured homodyne voltage is therefore a  $\pi/2$  rotation out-of-phase with the measured power, and the homodyne voltage is zero when a single photon is generated, as there is complete phase uncertainty in a photon Fock state.

Both the power and voltage of the photon output match the qubit state, demonstrating the ability to generate single photons, as well as arbitrary superpositions of zero and one photon, simply by controlling the qubit. Moreover, the amplitude of the pulse is as expected. The measured control pulse is used to calibrate the amplitude of the spontaneous emission. The frequency of qubit oscillations and a measurement of the control pulse on the output of the cavity together yield a calibration for the gain of the amplifiers, which in turn allows us to determine the efficiency of our single photon source. Simulations that include non-radiative channels of decay and

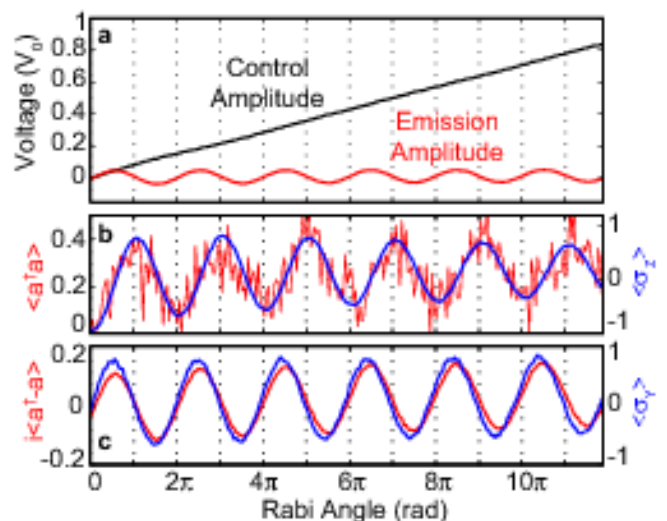


FIG. 3: Output of a single photon source. **a.** Measured drive and spontaneous emission voltage of cavity output, in units of zero-point voltage fluctuations  $V_0 \approx 2 \mu\text{V}$ . When the amplitude of the drive rotating the qubit is linearly increased, the output voltage of the cavity is oscillatory. **b.** Output power of the cavity  $\langle a^\dagger a \rangle$  detected with a diode (left axis), and the measured qubit state  $\langle \sigma_z \rangle$  (right axis). These peak when the qubit is in the excited state, after a  $\pi$  pulse; the agreement between qubit and photon states verifies the photon generation occurs as expected. The power collected after a 36 ns delay is 38% of a single photon. Fits to the qubit decays at later times are used to extrapolate the qubit polarization immediately after the control pulse. **c.** Average voltage of the output photons  $i\langle a^\dagger - a \rangle$  compared with the qubit state  $\langle \sigma_y \rangle$  measured with a Ramsey experiment. The agreement shows that the phase of superposition states is also transferred from qubit to photon. Only 12% of the voltage for the superposition is collected here, due non-radiative decay and dephasing during the 36 ns delay after the control pulse. The qubit amplitude is again extrapolated to the time immediately following the control pulse.

dephasing agree well with the observed data (see Figure 4), indicating that the power and amplitude of the source are well understood.

Using this calibration technique and Markovian master equation simulations, the complete time dynamics can be predicted to excellent accuracy, as shown for the homodyne voltage in Figure 4. Several features of the time dynamics are striking. First, because the control pulse sets the rotation axis, and the qubit state sets the emission phase, the control and generated photons are orthogonal in phase, which allows the two signals to be completely separated in homodyne detection. In the generated photon quadrature, rapid time oscillations are apparent during the control pulse; this is a direct observation of the Rabi oscillation of the qubit through its spontaneous emission. After the pulse, the qubit emits with a phase depending on its final state, resulting in oscillations in the control amplitude that smoothly connect to the time oscillations. Finally, there is a very low frequency oscillation in time. Photons are emitted at the qubit frequency, which is slightly detuned from the drive frequency. The result is a beating, with a half period

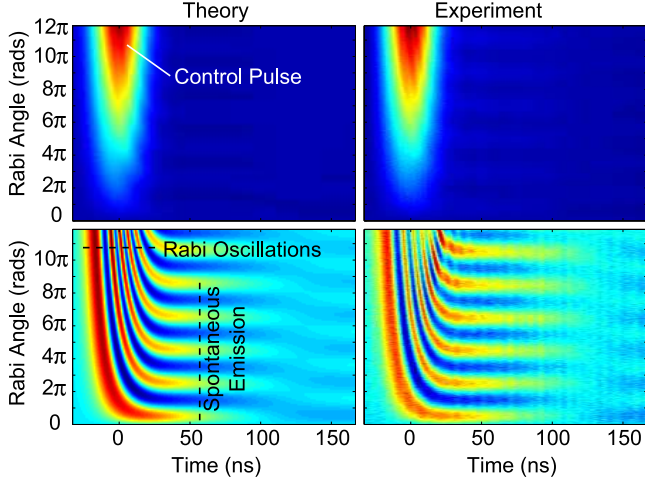


FIG. 4: Direct observation of the free induction decay of a superconducting qubit. Theoretical predictions (left) for both quadratures of the homodyne voltage, both in-phase (top) and out-of-phase (bottom) with the drive, agree well with experimental measurements of the two phases (right). Because emission is always orthogonal to the rotation axis, the spontaneous emission and control signal are phase separable. The homodyne sine waves in Figure 3 represent an integral of vertical slices through the emission. The frequency of these oscillations, coupled with a gain known from measurements of the control pulse, provide a calibration, which is used to predict the experimental emission data. Since the qubit and drive are slightly detuned by a fluctuating amount due to flux instability (on the order of 3 MHz), there is a slow beat note in the time direction. This fluctuating detuning is modeled by adding the predicted homodyne emission at two detunings,  $\pm 1.5$  MHz. The fast oscillations in the time domain are a direct measure of the Rabi oscillations of the qubit.

shown in both theory and data images, indicative of a frequency separation between the input and output photons in addition to the phase and time separations.

Two metrics of efficiency characterize the performance of the system. The source efficiency is the fraction of time in which a photon is emitted after a control pulse. This depends on the final polarization of the qubit and the ratio of radiative to non-radiative channels. In generating a single photon, the  $\pi$ -pulse leaves the qubit 87% polarized, and nearly all decay is radiative, giving source efficiency close to 87%. For generating a superposition of zero and one photon, the quadrature phase of the photon must also be controlled. Here, the qubit is 77% polarized along  $\sigma_y$ , but a dephasing rate  $\gamma_\phi = 1$  MHz leads to only  $\gamma_\kappa / (2\gamma_\phi + \gamma_\kappa) = 50\%$  radiation efficiency, giving a total source efficiency of 39%.

A second metric, the *usable* source efficiency, is somewhat lower in the current experiment, as the control pulse is slow and a delay is necessary to reject any control photons which could give a double-photon event. In the data of Figure 3, collection of radiation begins after 3 standard deviations of the control pulse Gaussian, making the likelihood of a control photon less than 0.01%. Integrating the measured spontaneous emission, the number of detected photons is measured directly, yielding an efficiency of 38% for the single photon source, and 12% for the homodyne voltage of the superposition state, which is again lower due to dephasing. Even rejecting the emission contaminated by control pulse photons, which contains the high signal-to-noise part of the emission, a substantial fraction of one photon is recovered. If a less stringent rejection threshold of 1% is chosen, efficiencies rise to 46% for power and 16% for homodyne voltage. In future experiments, this could be improved further with faster

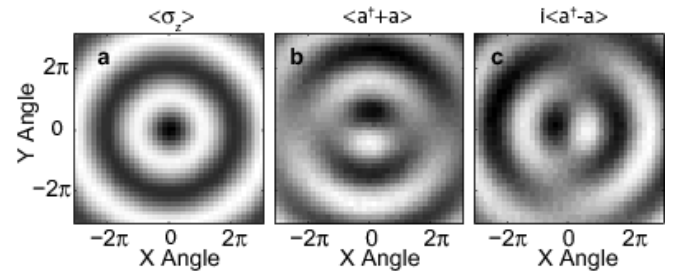


FIG. 5: Mapping the qubit state onto the photon state. **a.** Measurement of qubit state  $\langle \sigma_z \rangle$  after rotations by pulses of arbitrary amplitude and phase. Regardless of the phase of the pulse, the qubit oscillates to a peak after a  $\pi$  pulse. **b** and **c.** Fluorescence tomography. The amplitude of the voltage measured in each homodyne quadrature,  $\langle a + a^\dagger \rangle$  and  $i \langle a^\dagger - a \rangle$ , agree with expectations for  $\langle \sigma_x \rangle$  and  $\langle \sigma_y \rangle$ . Oscillations around the x-axis produce a signal in  $i \langle a^\dagger - a \rangle$  and none in  $\langle a + a^\dagger \rangle$ . This shows the ability to map an arbitrary qubit state onto a photon state, as well as the ability to characterize a qubit state through spontaneous emission.



pulses, longer coherence times, or fast tunability of the qubit frequency, achieving usable source efficiencies close to 100%.

Tomography presents an even more powerful tool for characterizing the qubit[28] and photon states[29, 30], and demonstrates the complete mapping of the qubit state onto the photons (Figure 5). Here, qubit tomography is performed by applying control pulses of arbitrary phase and amplitude, and performing a dispersive measurement of the qubit state  $\langle\sigma_z\rangle$ . This yields the expected concentric rings for a qubit initially in the ground state (Figure 5a). A fluorescence homodyne tomography technique is used to characterize the photons. Control pulses with all phases and amplitudes are applied, and both quadratures of the output homodyne voltage are recorded (Figures 5b and 5c). These show excellent agreement with the expected  $\sigma_x$  and  $\sigma_y$  components of the qubit state[28]. This fluorescence tomography technique allows a full characterization of the qubit by looking at the spontaneous emission at the output, directly observing a superconducting qubit at its Larmor frequency. Moreover, this means that a qubit state can be transferred onto a photon state, thus moving information from a stationary qubit to a “flying qubit”, one of the DiVincenzo resources for quantum information processing[2].

The mapping of qubit states onto photon states allows for the use of microwave photons as a true resource for quantum information on a chip. These photons are generated on-demand with a high repetition rate, good spectral purity, and high efficiency. This is a convenient means of creating non-classical states of light to interact with atoms, all in the wires of an integrated circuit, allowing them to be shuttled around a chip. The generation of single photons, and superpositions of photon states, is an important step towards on-chip quantum optics experiments.

- 
- [1] Schuster, D. I. *et al.* Resolving photon number states in a superconducting circuit. *Nature* **445**, 515–518 (2007).
  - [2] DiVincenzo, D. P. The physical implementation of quantum computation. *Fortschritte der Physik* **48**, 771–783 (2000).
  - [3] Blais, A., Huang, R.-S., Wallraff, A., Girvin, S. M. & Schoelkopf, R. J. Cavity quantum electrodynamics for superconducting electrical circuits: An architecture for quantum computation. *Phys. Rev. A* **69**, 062320–14 (2004).
  - [4] Oxborrow, M. & Sinclair, A. Single-photon sources. *Contemporary Physics* **46**, 173–206 (2005).
  - [5] Clauser, J. F. Experimental distinction between the quantum and classical field-theoretic predictions for the photoelectric effect. *Phys. Rev. D* **9**, 853– (1974).
  - [6] Kimble, H. J., Dagenais, M. & Mandel, L. Photon antibunching in resonance fluorescence. *Phys. Rev. Lett.* **39**, 691– (1977).
  - [7] Diedrich, F. & Walther, H. Nonclassical radiation of a single stored ion. *Phys. Rev. Lett.* **58**, 203– (1987).
  - [8] Darquie, B. *et al.* Controlled single-photon emission from a single trapped two-level atom. *Science* **309**, 454–456 (2005).
  - [9] Basche, T., Moerner, W. E., Orrit, M. & Talon, H. Photon antibunching in the fluorescence of a single dye molecule trapped in a solid. *Phys. Rev. Lett.* **69**, 1516– (1992).
  - [10] Brunel, C., Lounis, B., Tamarat, P. & Orrit, M. Triggered source of single photons based on controlled single molecule fluorescence. *Phys. Rev. Lett.* **83**, 2722– (1999).
  - [11] Lounis, B. & Moerner, W. E. Single photons on demand from a single molecule at room temperature. *Nature* **407**, 491–493 (2000).
  - [12] Kurtsiefer, C., Mayer, S., Zarda, P. & Weinfurter, H. Stable solid-state source of single photons. *Phys. Rev. Lett.* **85**, 290– (2000).
  - [13] Michler, P. *et al.* Quantum correlation among photons from a single quantum dot at room temperature. *Nature* **406**, 968–970 (2000).
  - [14] Pelton, M. *et al.* Efficient source of single photons: A single quantum dot in a micropost microcavity. *Phys. Rev. Lett.* **89**, 233602– (2002).
  - [15] Purcell, E. M. Spontaneous emission probabilities at radio frequencies. *Physical Review* **69**, 681 (1946).
  - [16] Brattke, S., Varcoe, B. T. H. & Walther, H. Generation of photon number states on demand via cavity quantum electrodynamics. *Phys. Rev. Lett.* **86**, 3534– (2001).
  - [17] Kuhn, A., Hennrich, M. & Rempe, G. Deterministic single-photon source for distributed quantum networking. *Phys. Rev. Lett.* **89**, 067901– (2002).
  - [18] McKeever, J. *et al.* Deterministic generation of single photons from one atom trapped in a cavity. *Science* **303**, 1992–1994 (2004).
  - [19] Maitre, X. *et al.* Quantum memory with a single photon in a cavity. *Phys. Rev. Lett.* **79**, 769– (1997).
  - [20] Keller, M., Lange, B., Hayasaka, K., Lange, W. & Walther, H. Continuous generation of single photons with controlled waveform in an ion-trap cavity system. *Nature* **431**, 1075–1078 (2004).
  - [21] Moreau, E. *et al.* Single-mode solid-state single photon source based on isolated quantum dots in pillar microcavities. *Appl. Phys. Lett.* **79**, 2865–2867 (2001).
  - [22] Santori, C., Fattal, D., Vuckovic, J., Solomon, G. S. & Yamamoto, Y. Indistinguishable photons from a single-photon device. *Nature* **419**, 594–597 (2002).
  - [23] Wallraff, A. *et al.* Strong coupling of a single photon to a superconducting qubit using circuit quantum electrodynamics. *Nature* **431**, 162–167 (2004).
  - [24] Chiorescu, I. *et al.* Coherent dynamics of a flux qubit coupled to a harmonic oscillator. *Nature* **431**, 159–162 (2004).
  - [25] Koch, J. *et al.* Optimizing the cooper pair box: Introducing the transmon. In preparation (2007).
  - [26] Bouchiat, V., Vion, D., Joyez, P., Esteve, D. & Devoret, M. H. Quantum coherence with a single cooper pair. *Physica Scripta* **T76**, 165–170 (1998).
  - [27] Wallraff, A. *et al.* Approaching unit visibility for control of a superconducting qubit with dispersive readout. *Phys. Rev. Lett.* **95**, 060501–4 (2005).
  - [28] Steffen, M. *et al.* State tomography of capacitively shunted phase qubits with high fidelity. *Phys. Rev. Lett.* **97**, 050502–4 (2006).

- [29] Smithey, D. T., Beck, M., Raymer, M. G. & Faridani, A. Measurement of the wigner distribution and the density matrix of a light mode using optical homodyne tomography: Application to squeezed states and the vacuum. *Phys. Rev. Lett.* **70**, 1244– (1993).
- [30] Leonhardt, U. *Measuring the Quantum State of Light* (Cambridge University Press, 1997).

This work was supported in part by the National Se-

curity Agency under the Army Research Office, the NSF, and Yale University. A.H. would like to acknowledge support from Yale University via a Quantum Information and Mesoscopic Physics Fellowship. The authors declare that they have no competing financial interests. Correspondence and requests for materials should be addressed to Rob Schoelkopf (email:Robert.Schoelkopf@yale.edu).